Turbulent Flows

Stephen B. Pope
Cambridge University Press, 2000

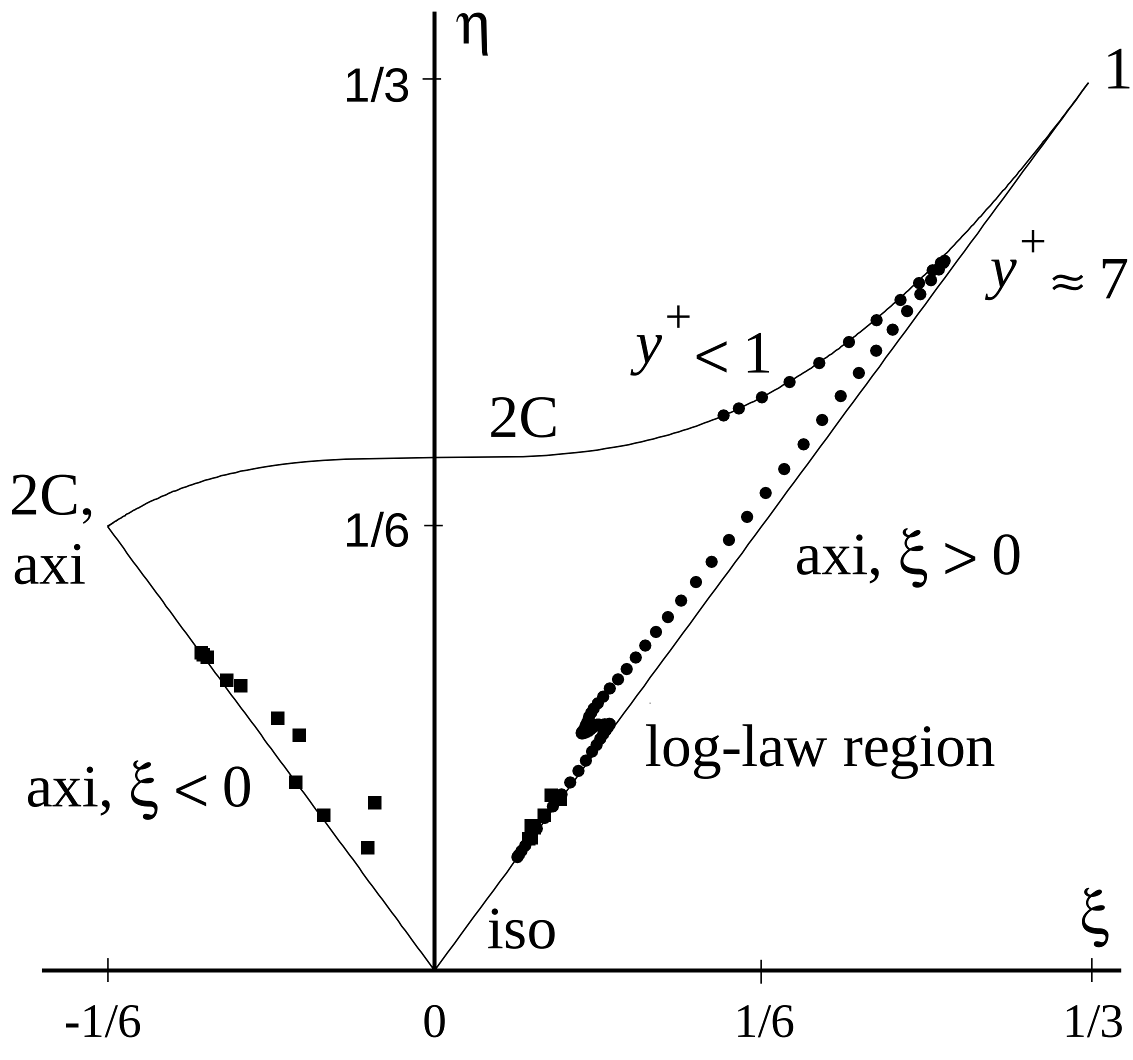

Figure 11.1: The Lumley triangle on the plane of the invariants ξ and η of the Reynolds-stress anisotropy tensor. The lines and vertices correspond to special states (see Table 11.1). Circles: from DNS of channel flow (Kim *et al.* 1987). Squares: from experiments on a turbulent mixing layer (Bell and Mehta 1990). 1C, one-component; 2C, two-component.

Turbulent Flows

Stephen B. Pope
Cambridge University Press, 2000

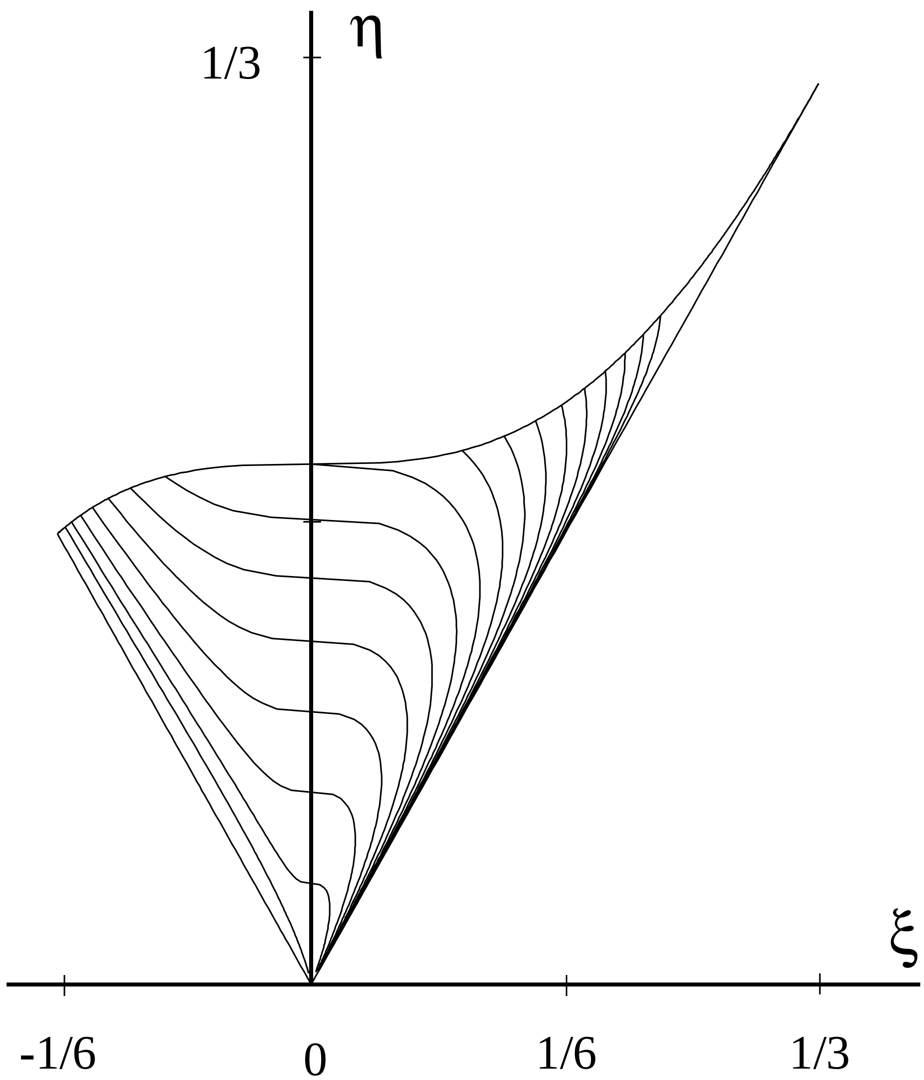

Figure 11.2: Trajectories on the ξ-η plane given by the model of Sarkar and Speziale (1990) (Eqs. 11.51 and 11.57).

Turbulent Flows

Stephen B. Pope
Cambridge University Press, 2000

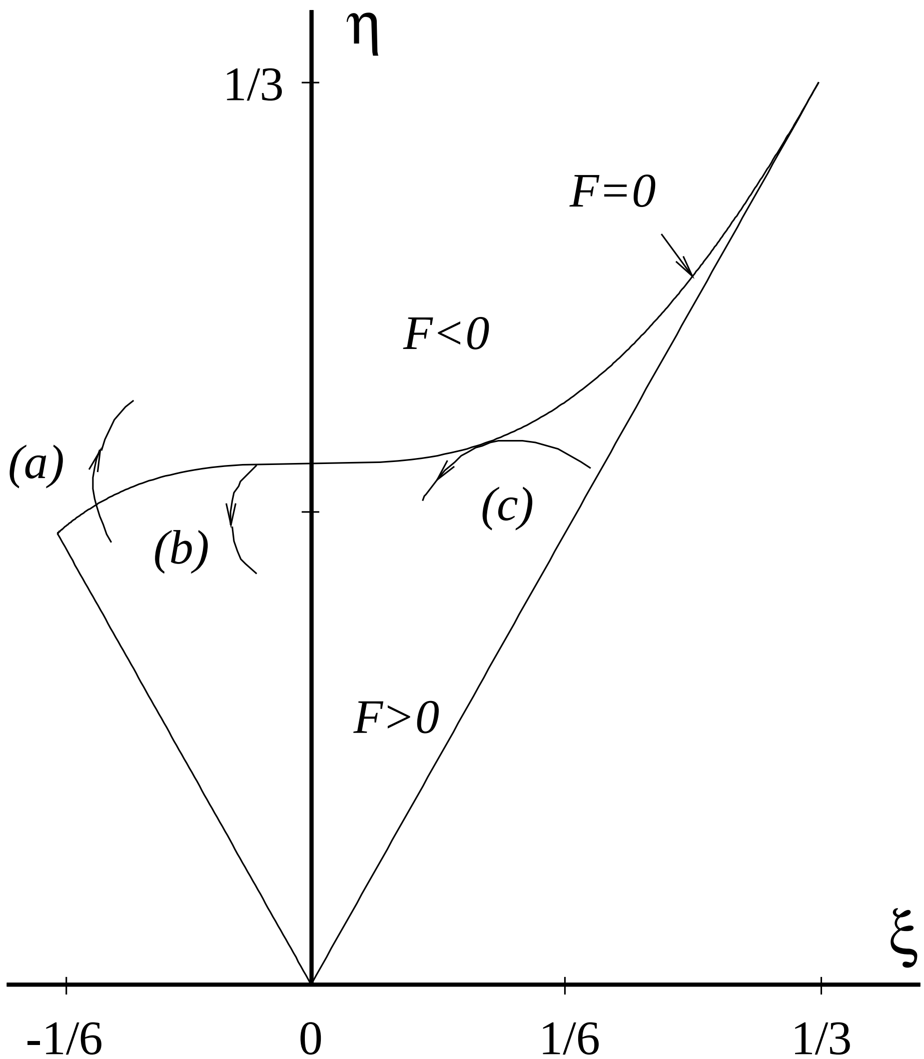

Figure 11.3: The Lumley triangle showing trajectories of three types: (a) violates realizability; (b) satisfies weak realizability; (c) satisfies strong realizability. (Note: other types of trajectories are possible.)

Turbulent Flows

Stephen B. Pope
Cambridge University Press, 2000

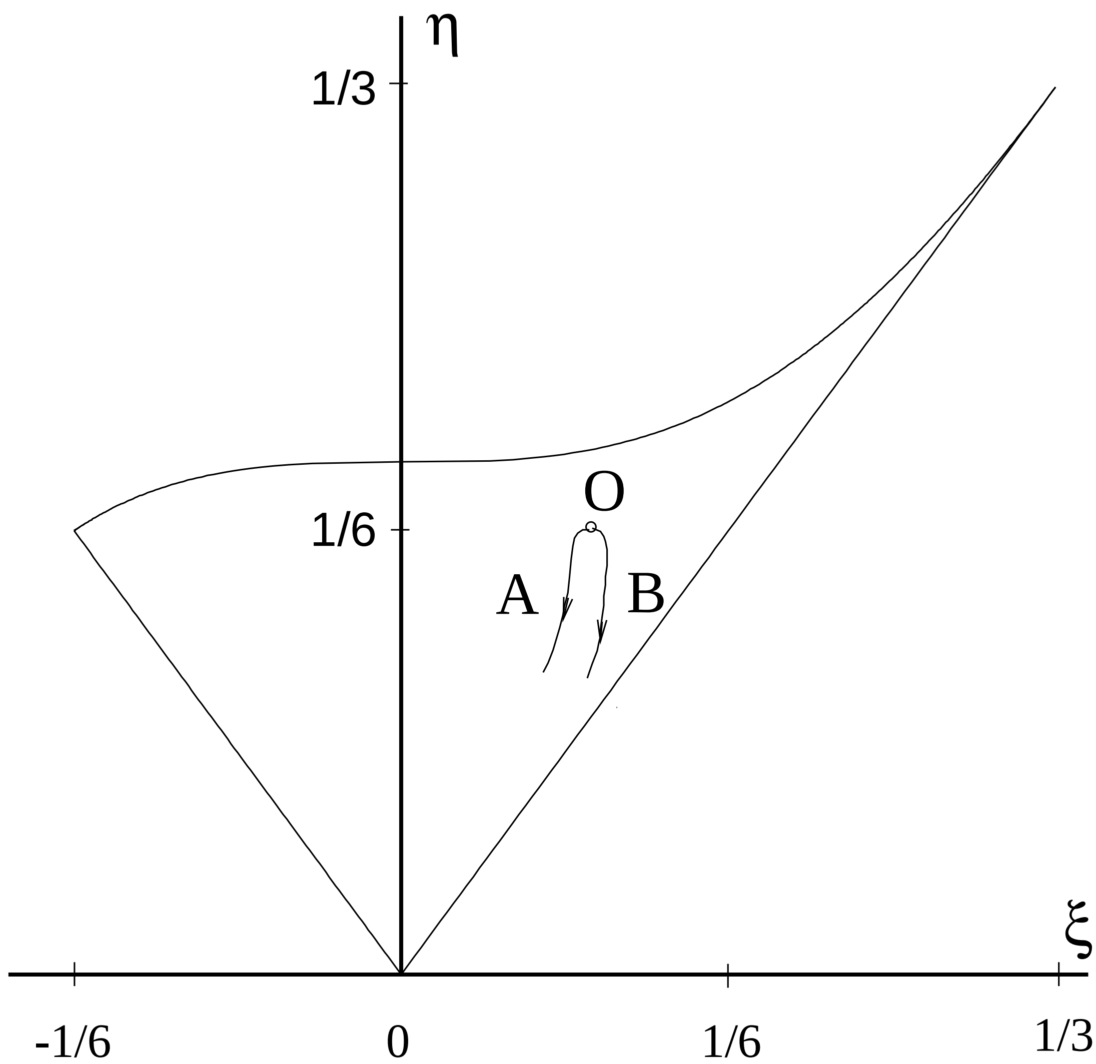

Figure 11.4: Sketch of trajectories (A and B) on the ξ-η plane for two experiments (or DNS) in which the initial spectra are different, but the initial values of **b** are the same. A Reynolds-stress model yields a unique trajectory from initial point O.

Turbulent Flows

Stephen B. Pope
Cambridge University Press, 2000

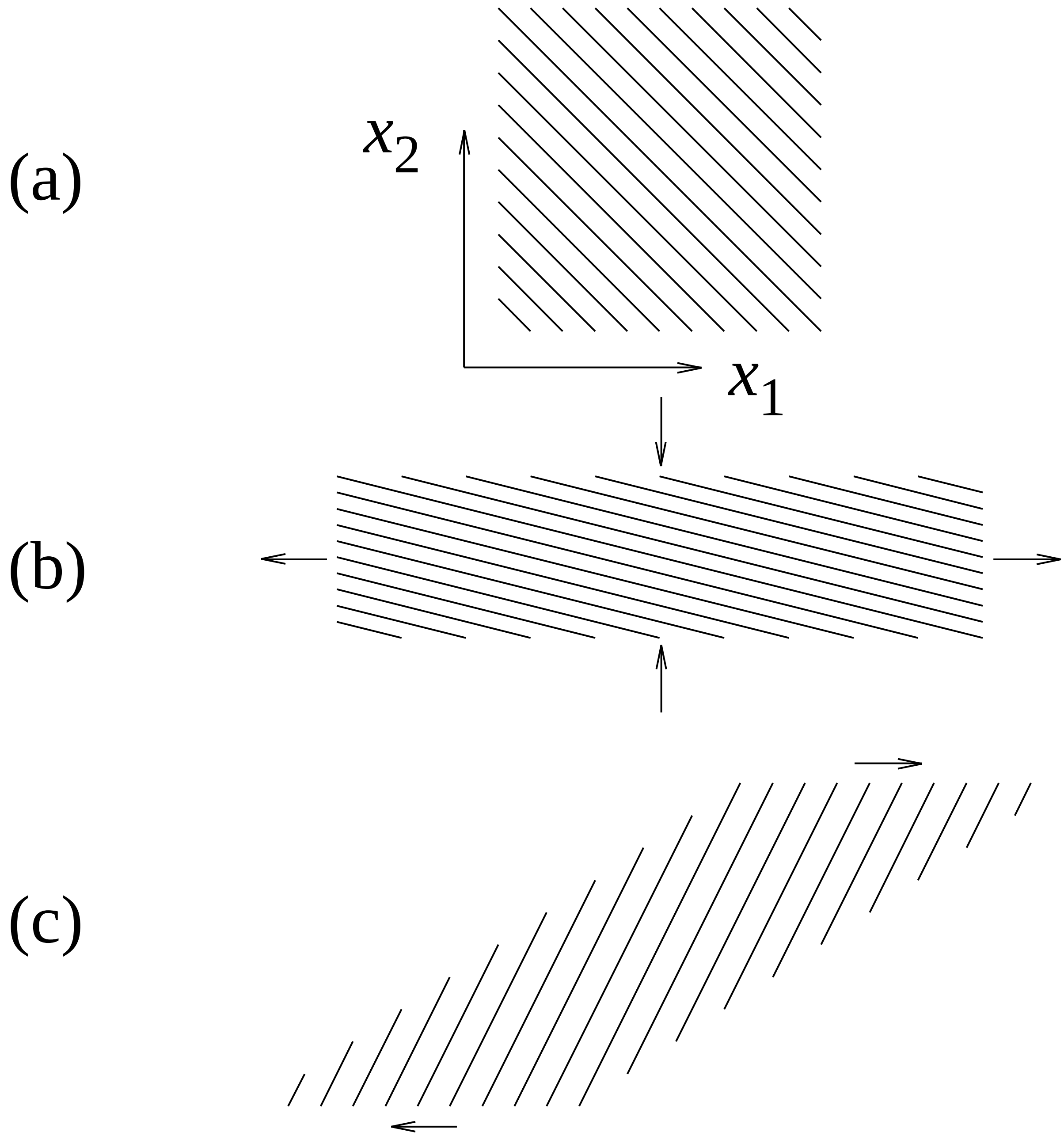

Figure 11.5: Crests of the fields $\boldsymbol{\phi}(\mathbf{x}, t)$ evolving by $\bar{\mathrm{D}}\phi/\bar{\mathrm{D}}t = 0$ (a) initial condition, $\phi e^{i\boldsymbol{\kappa}^o\cdot\mathbf{x}}$, $\kappa_1^o = \kappa_2^o > 0$, $\kappa_3^o = 0$ (b) after plane straining ($\bar{S}_{11} = -\bar{S}_{22} > 0$) (c) after shearing $\partial\langle U_1\rangle/\partial x_2 > 0$.

Turbulent Flows

Stephen B. Pope
Cambridge University Press, 2000

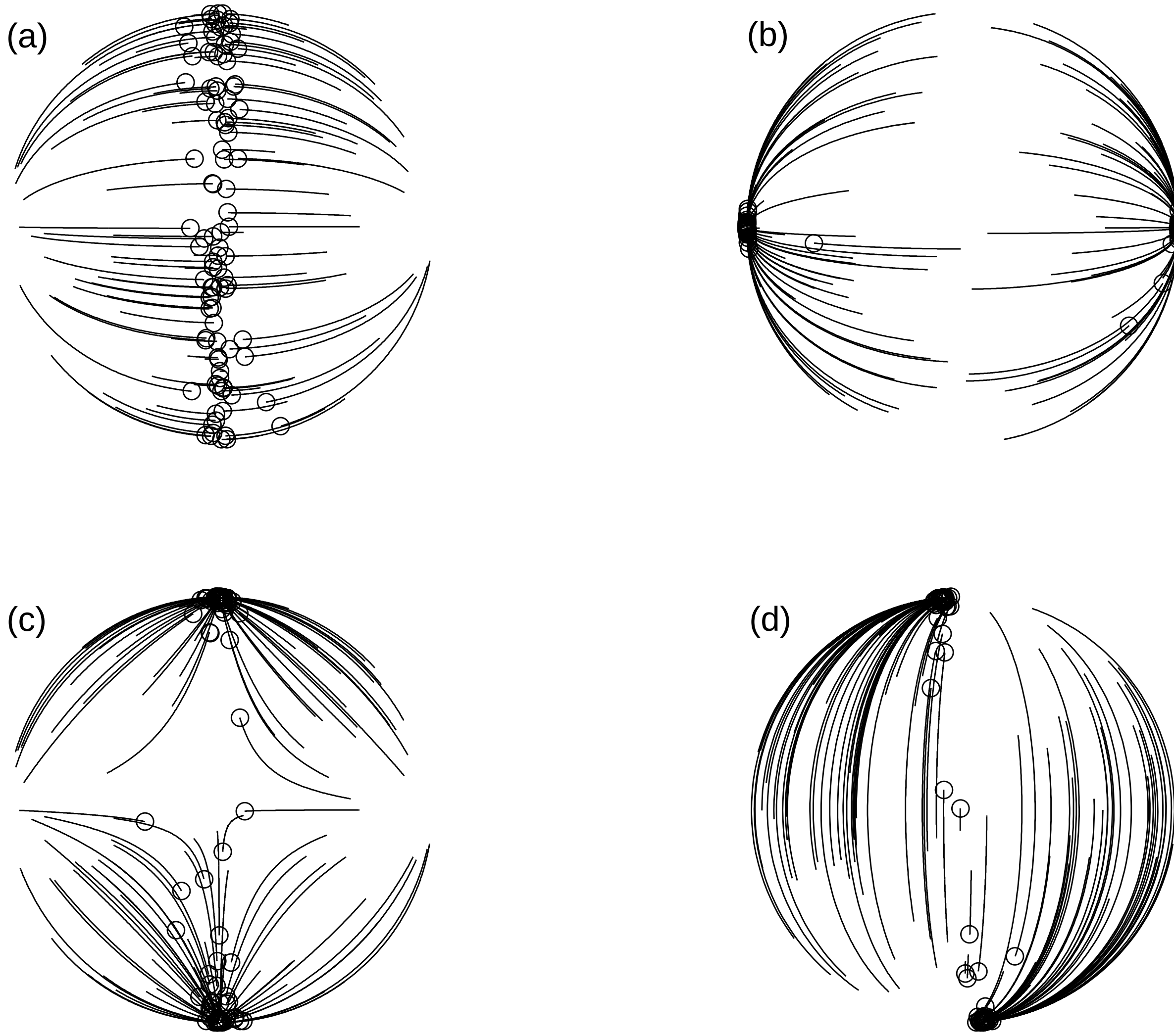

Figure 11.6: Trajectories of the unit wavevector $\hat{\mathbf{e}}(t)$ on the unit sphere from random initial conditions for (a) axisymmetric contraction (b) axisymmetric expansion (c) plane strain (d) shear. The $\hat{e}_1$ direction is horizontal, the $\hat{e}_2$ direction is vertical, and the $\hat{e}_3$ direction is into the page. The symbols mark the ends of the trajectories after distortion.

Turbulent Flows

Stephen B. Pope

Cambridge University Press, 2000

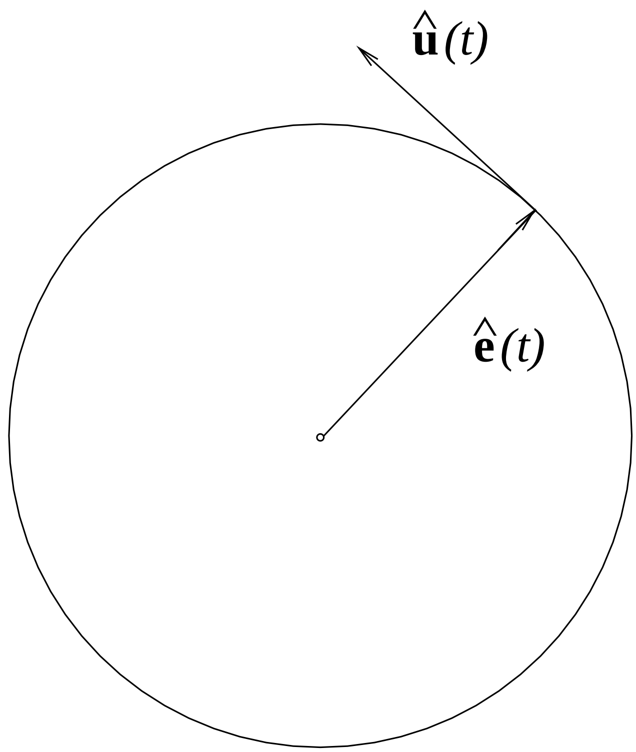

Figure 11.7: Sketch of the unit sphere showing the unit wavevector $\hat{\mathbf{e}}(t)$. The Fourier component of velocity $\hat{\mathbf{u}}(t)$ is orthogonal to $\hat{\mathbf{e}}(t)$, and so it is in the tangent plane of the unit sphere at $\hat{\mathbf{e}}(t)$.

Turbulent Flows

Stephen B. Pope
Cambridge University Press, 2000

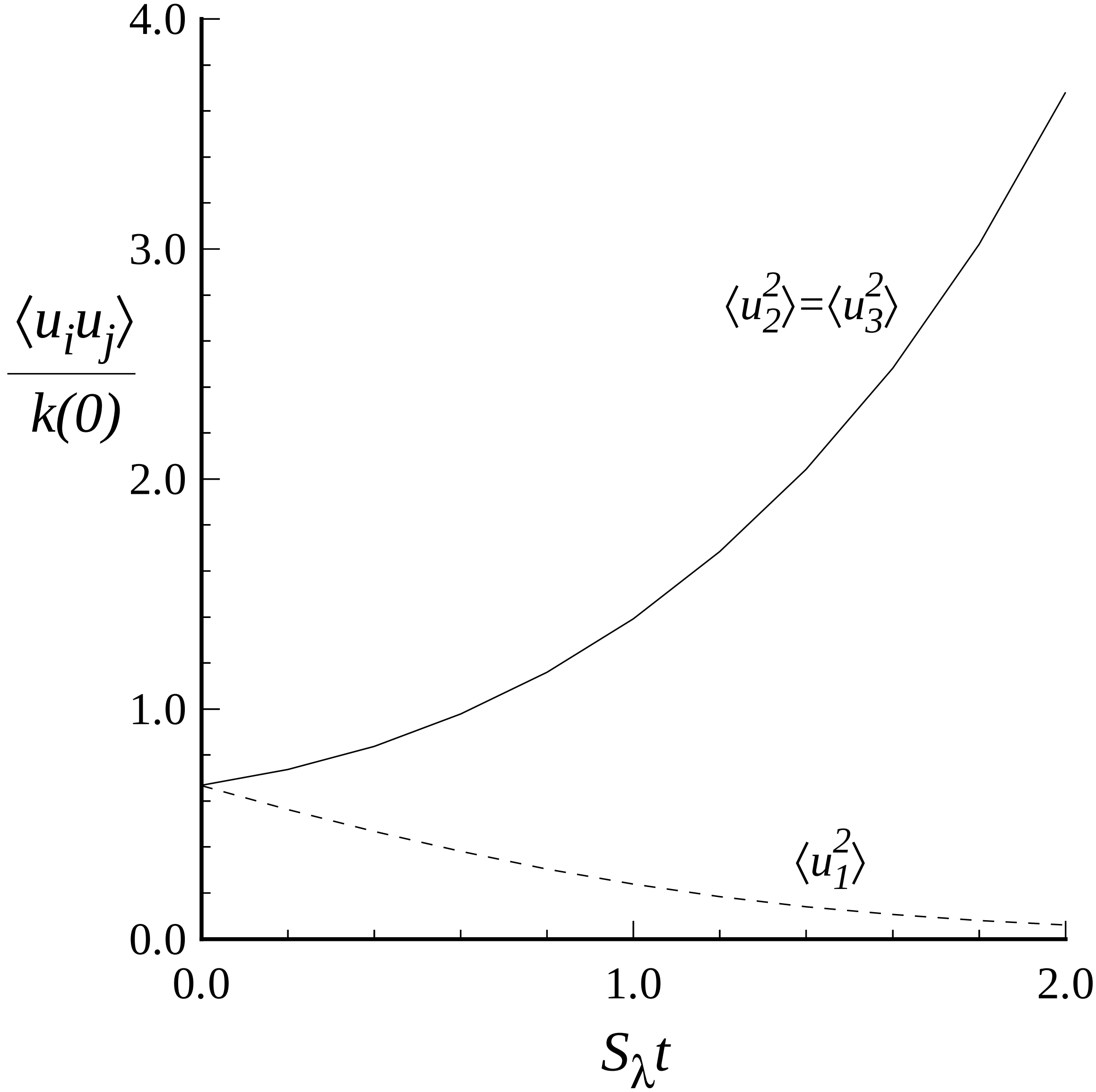

Figure 11.8: Sketch of the unit sphere showing the unit wavevector $\hat{\mathbf{e}}(t)$. The Fourier component of velocity $\hat{\mathbf{u}}(t)$ is orthogonal to $\hat{\mathbf{e}}(t)$, and so it is in the tangent plane of the unit sphere at $\hat{\mathbf{e}}(t)$.

Turbulent Flows

Stephen B. Pope

Cambridge University Press, 2000

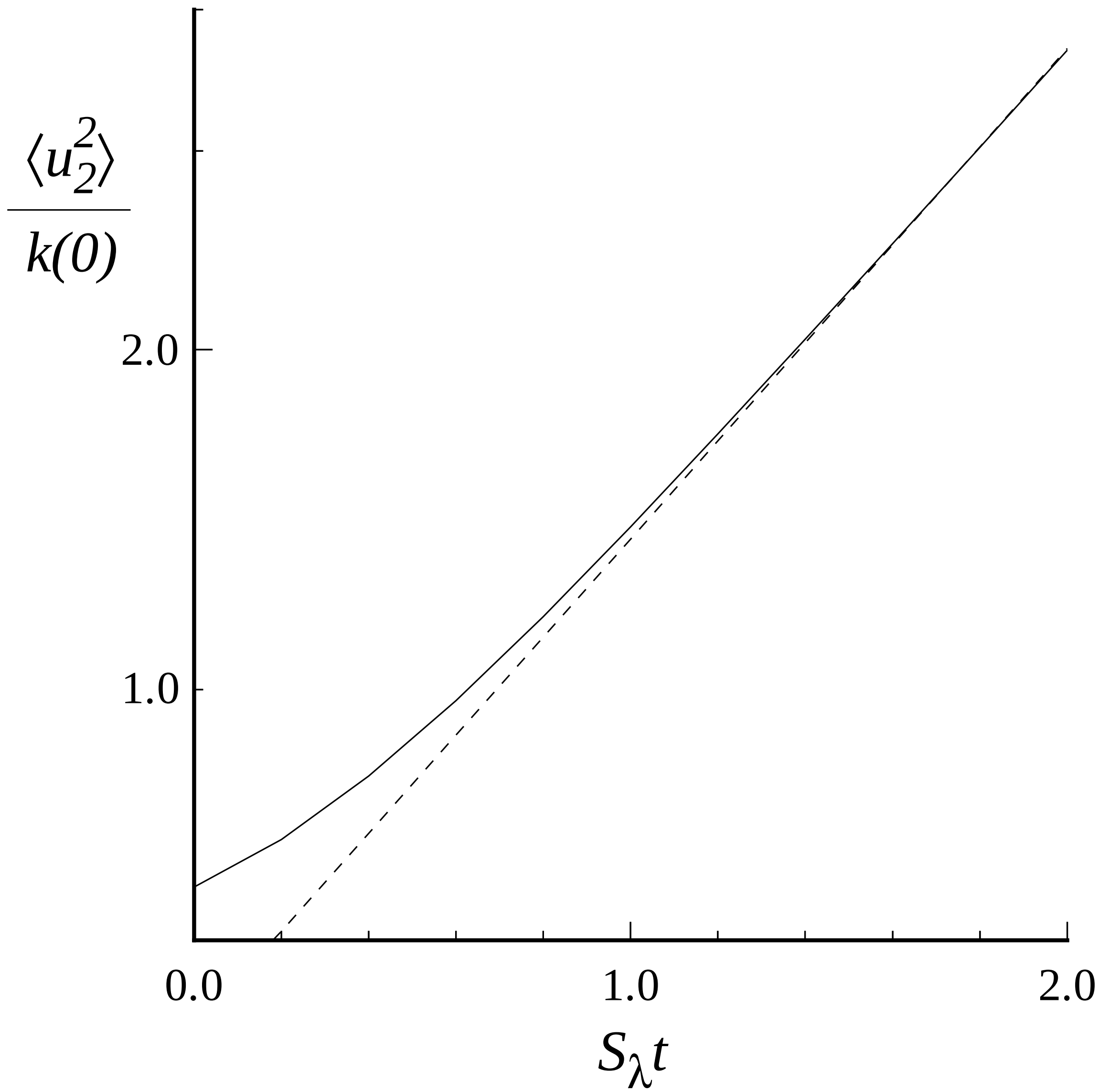

Figure 11.9: Evolution of $\langle u_2^2 \rangle$ (on a log scale) for axisymmetric contraction rapid distortion (solid line). The dashed line is $\frac{1}{2}\exp(\mathcal{S}_\lambda t)$ indicating the asymptotic growth rate.

Turbulent Flows

Stephen B. Pope
Cambridge University Press, 2000

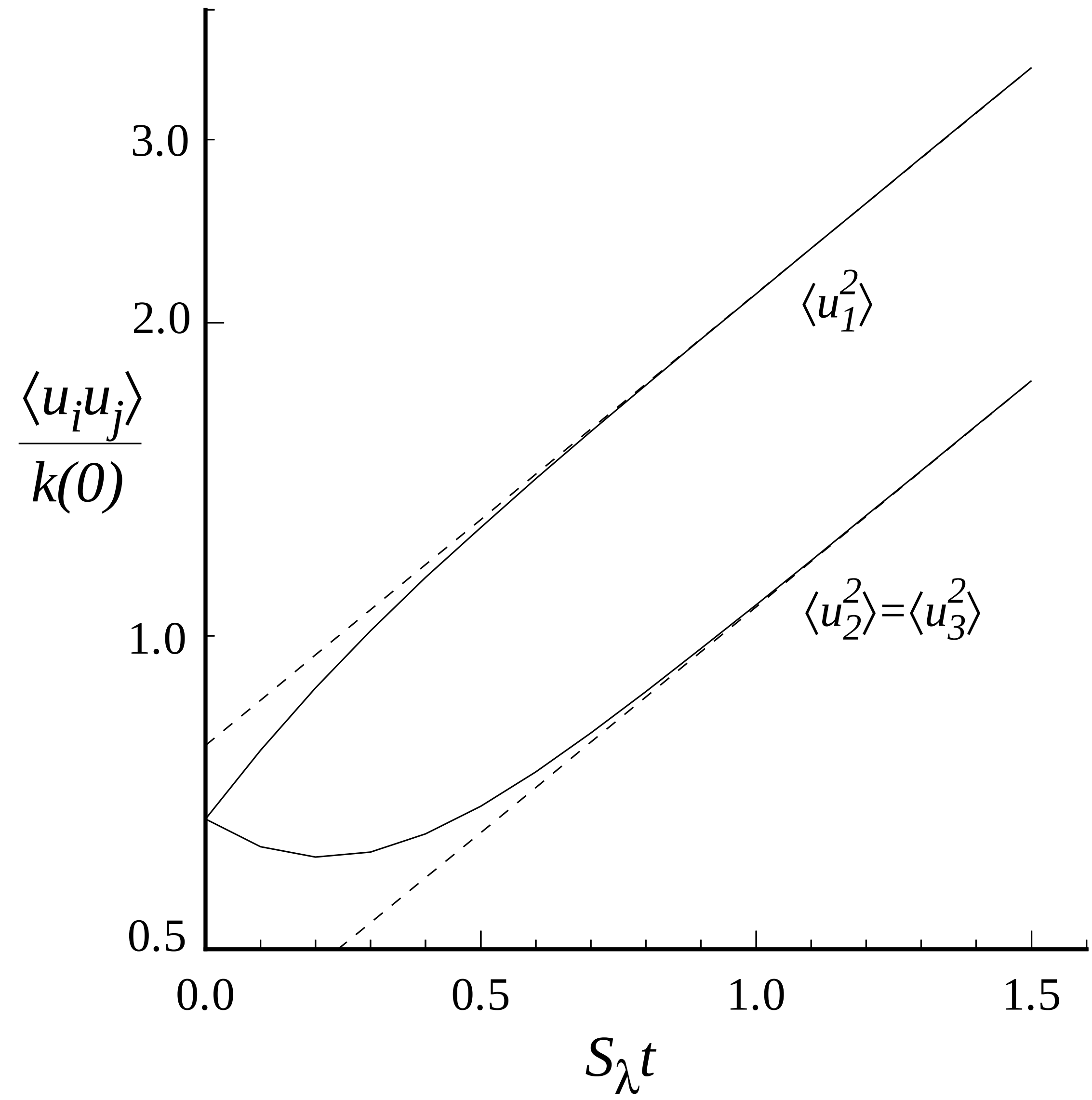

Figure 11.10: Evolution of Reynolds stresses for axisymmetric expansion rapid distortion. The dashed lines show the asymptotic growth as $\exp(\mathcal{S}_\lambda t)$.

Turbulent Flows

Stephen B. Pope
Cambridge University Press, 2000

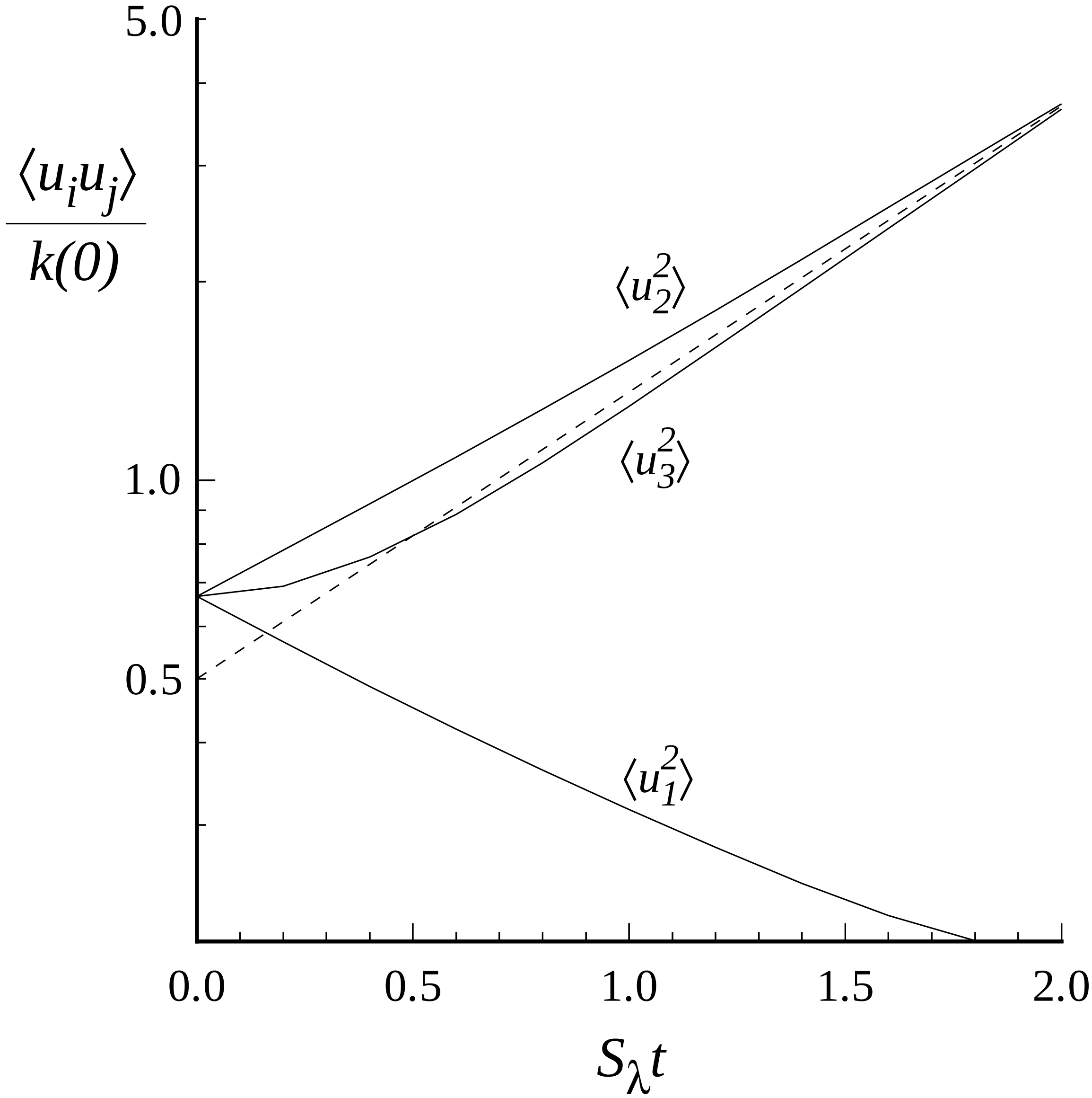

Figure 11.11: Evolution of Reynolds stresses for plane strain rapid distortion. The dashed line is $\frac{1}{2}\exp(\mathcal{S}_\lambda t)$.

Turbulent Flows

Stephen B. Pope
Cambridge University Press, 2000

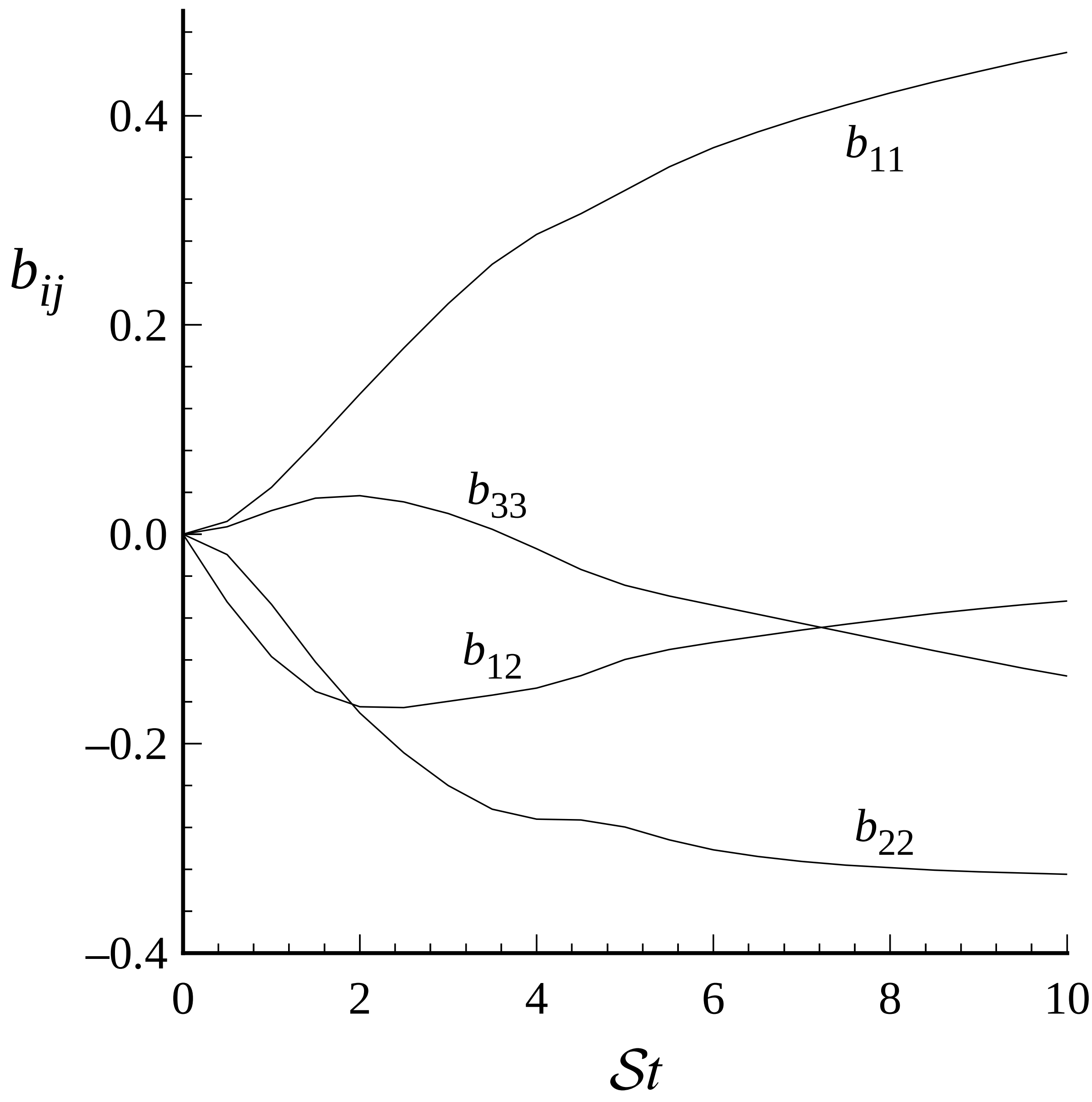

Figure 11.12: Evolution of Reynolds-stress anisotropies for shear rapid distortion.

Turbulent Flows

Stephen B. Pope
Cambridge University Press, 2000

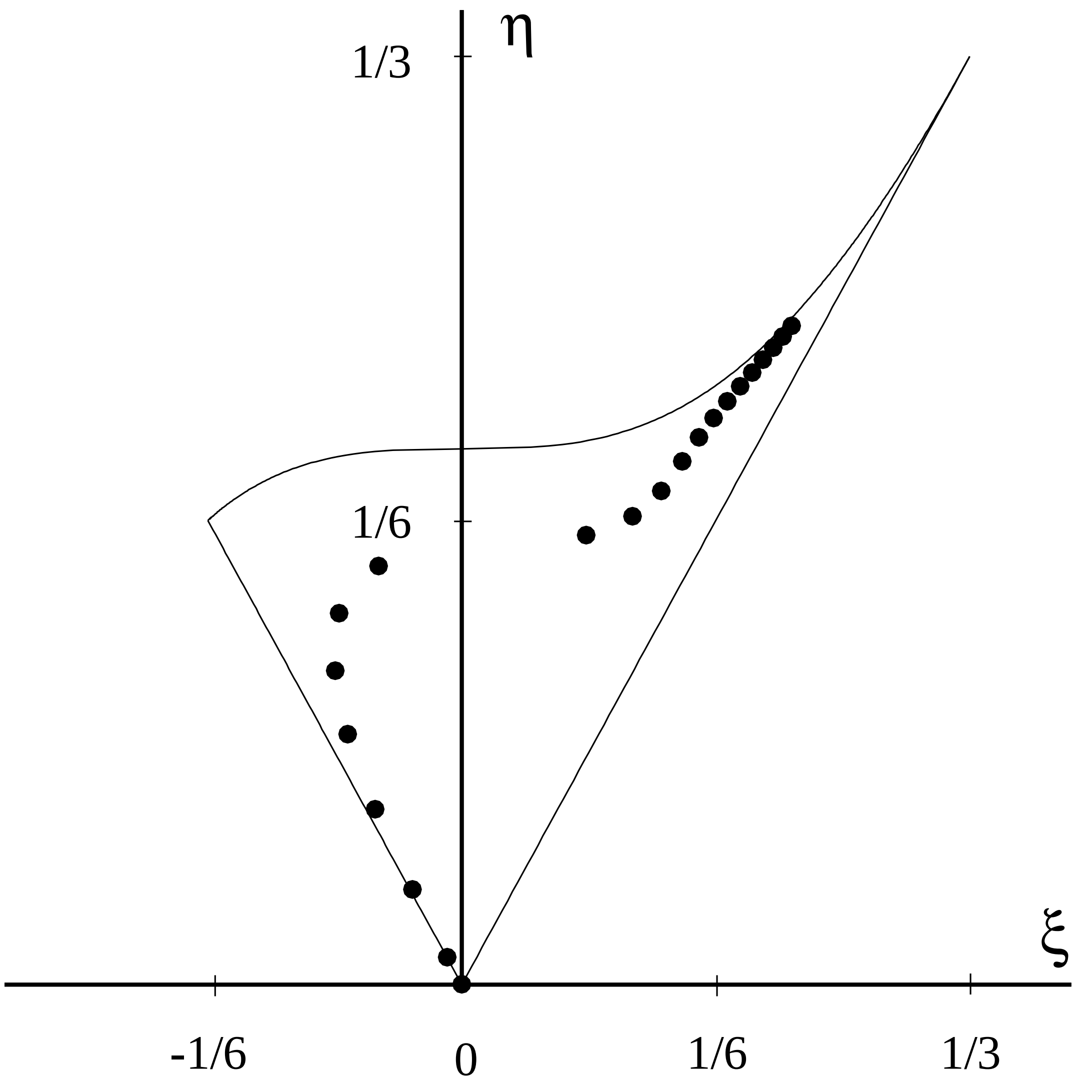

Figure 11.13: Evolution of the Reynolds-stress invariants for shear rapid distortion. Starting from the origin (corresponding to isotropy), each symbol gives the state after an amount of shear $\mathcal{S}t = 0.5$.

Turbulent Flows

Stephen B. Pope
Cambridge University Press, 2000

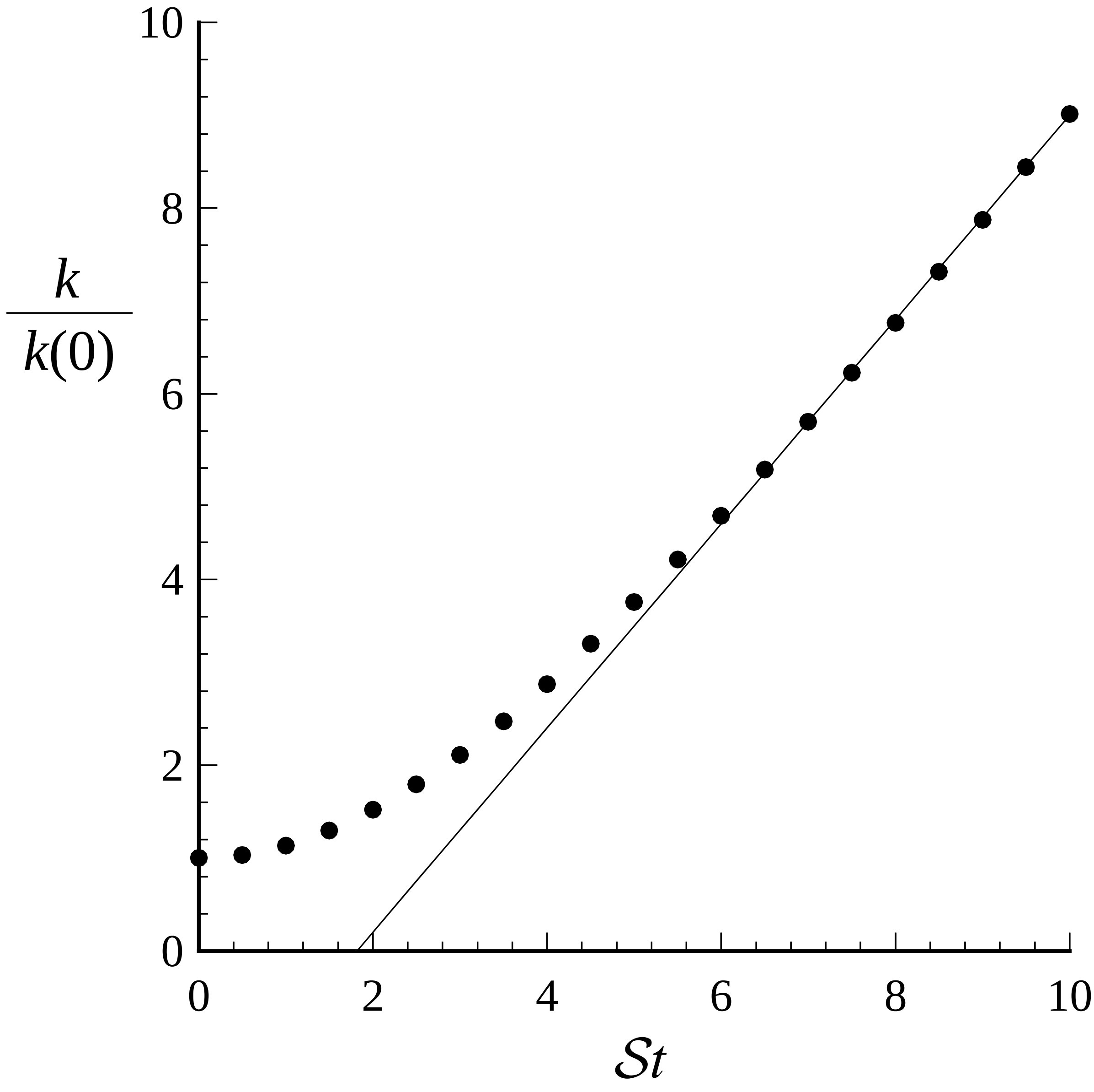

Figure 11.14: Evolution of the turbulent kinetic energy for shear rapid distortion.

Turbulent Flows

Stephen B. Pope
Cambridge University Press, 2000

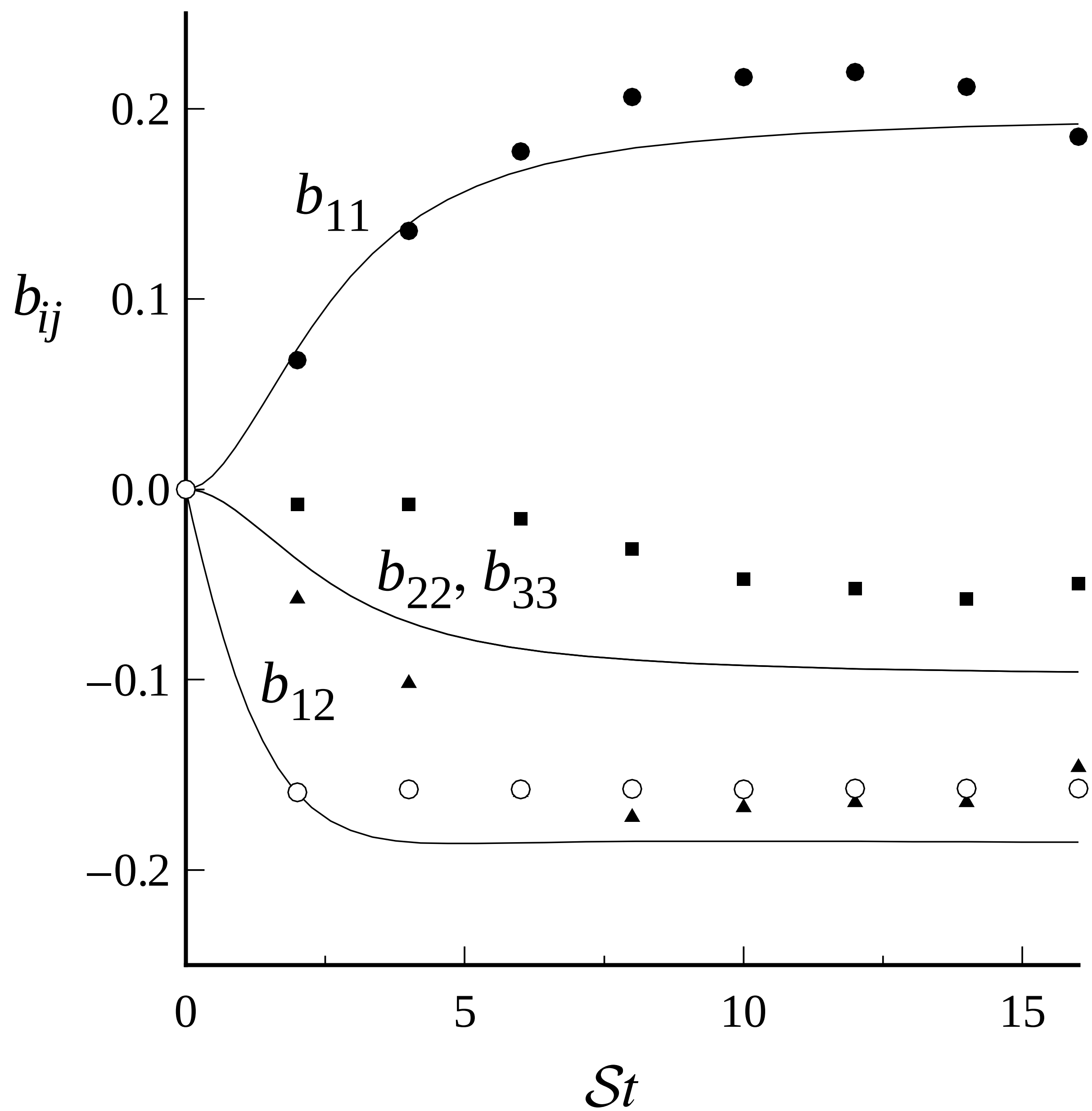

Figure 11.15: Reynolds-stress anisotropies in homogeneous shear flow. Comparison of LRR-IP model calculations (lines) with the DNS data of Rogers Moin (1987) (symbols): •, b_{11}; ∘, b_{12}; squares, b_{22}; triangles, b_{33}.

Turbulent Flows

Stephen B. Pope
Cambridge University Press, 2000

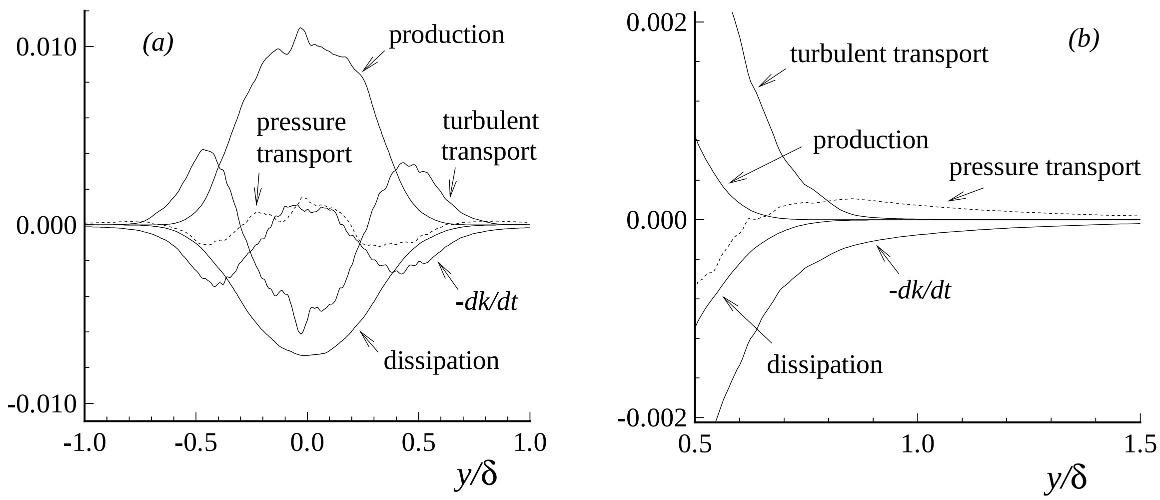

Figure 11.16: Kinetic energy budget in the temporal mixing layer from the DNS data of Rogers and Moin (1994): (a) across the whole flow (b) an expanded view of the edge of the layer. The contributions to the budget are: production $\mathcal{P}$; dissipation $-\varepsilon$; rate of change $-\mathrm{d}k/\mathrm{d}t$; turbulent transport; pressure transport (dashed line). All quantities are normalized by the velocity difference and the layer thickness δ (see Fig. 5.21).

Turbulent Flows

Stephen B. Pope
Cambridge University Press, 2000

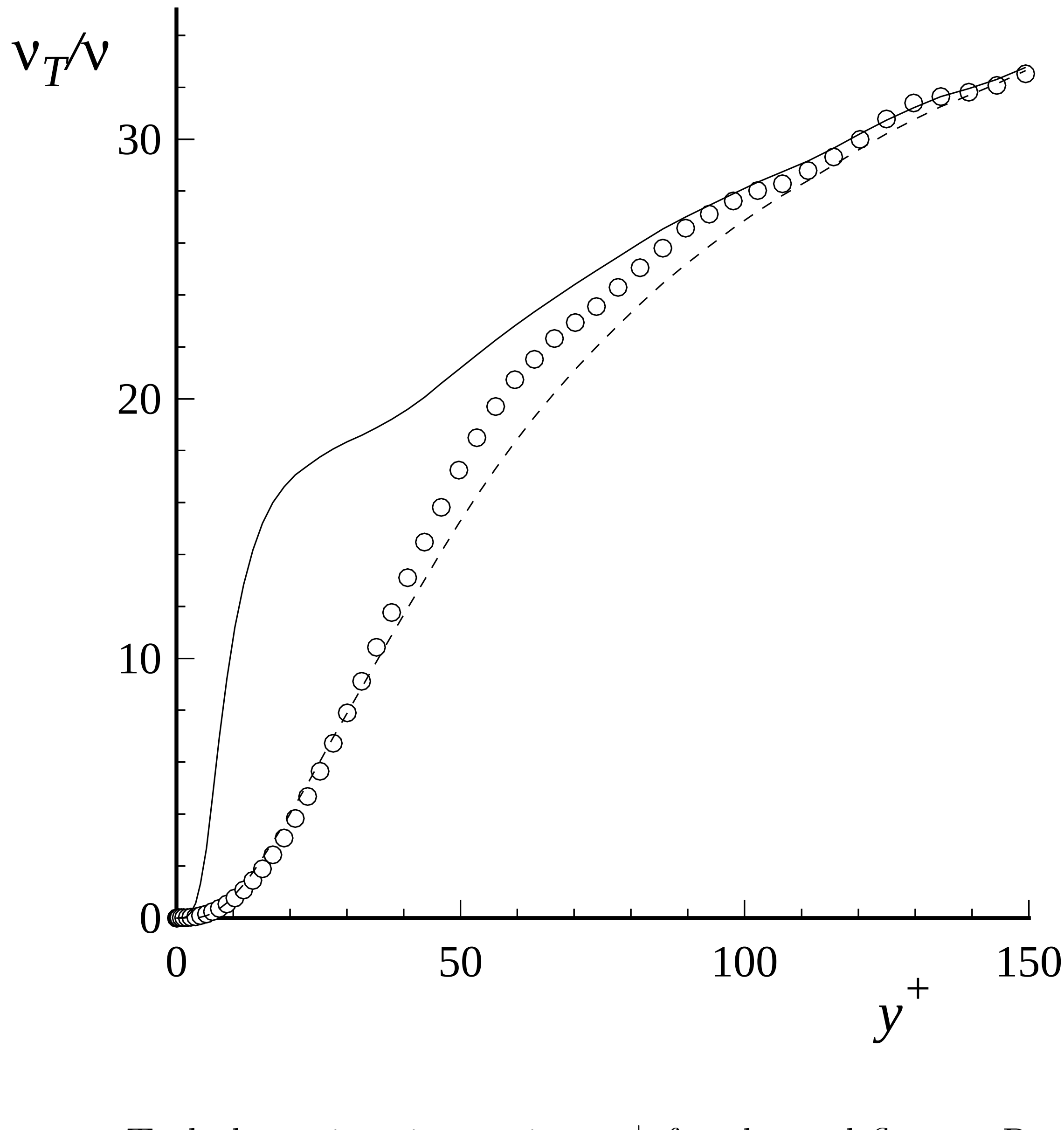

Figure 11.17: Turbulent viscosity against y^+ for channel flow at Re = 13,750. Symbols, DNS data of Kim *et al.* (1987); solid line, $0.09k^2/\varepsilon$; dashed line, $0.22\langle v^2\rangle k/\varepsilon$.

Turbulent Flows

Stephen B. Pope
Cambridge University Press, 2000

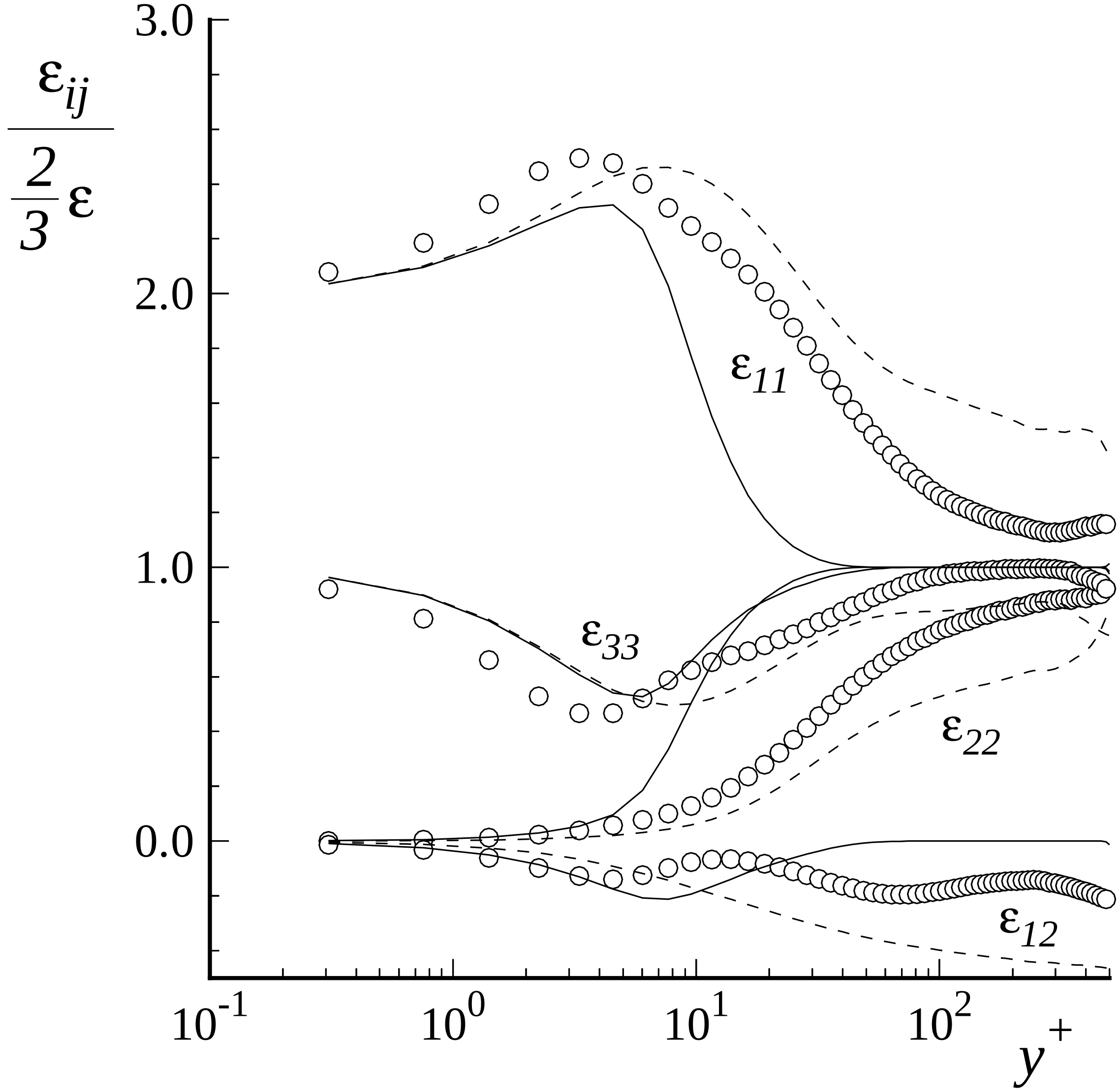

Figure 11.18: Normalized dissipation components in a turbulent boundary layer at $\text{Re}_\theta = 1,410$: symbols, DNS data of Spalart (1988); dashed lines, Rotta's model, Eq. (11.167); solid lines, Eq. (11.169).

Turbulent Flows

Stephen B. Pope
Cambridge University Press, 2000

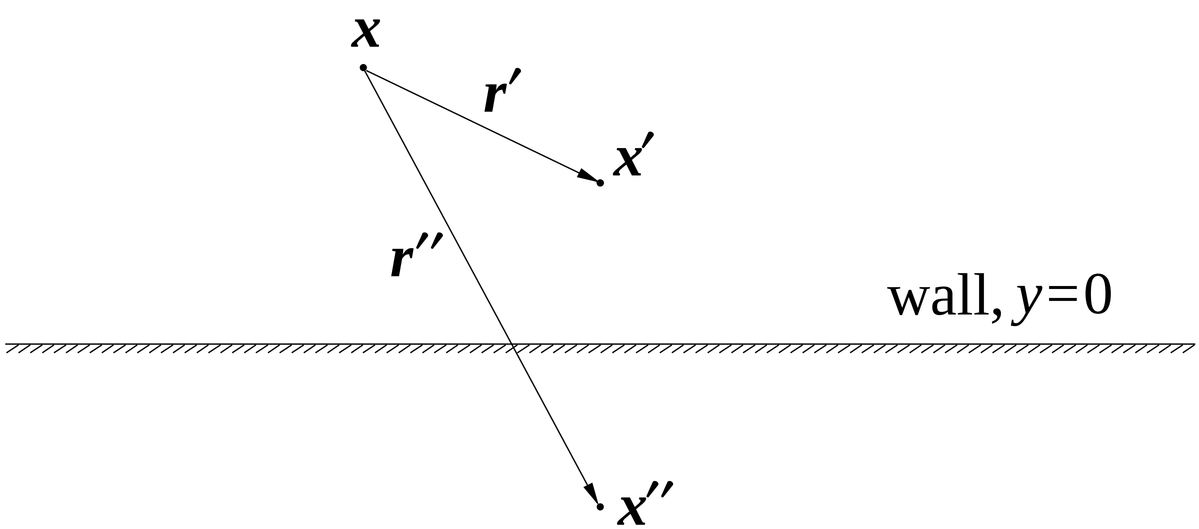

Figure 11.19: Sketch of the point $\mathbf{x}'$ and its image $\mathbf{x}''$, showing the vectors $\mathbf{r}'$ and $\mathbf{r}''$ that appear in the Green's function solutions, Eqs. (11.181) and (11.182).

Turbulent Flows

Stephen B. Pope
Cambridge University Press, 2000

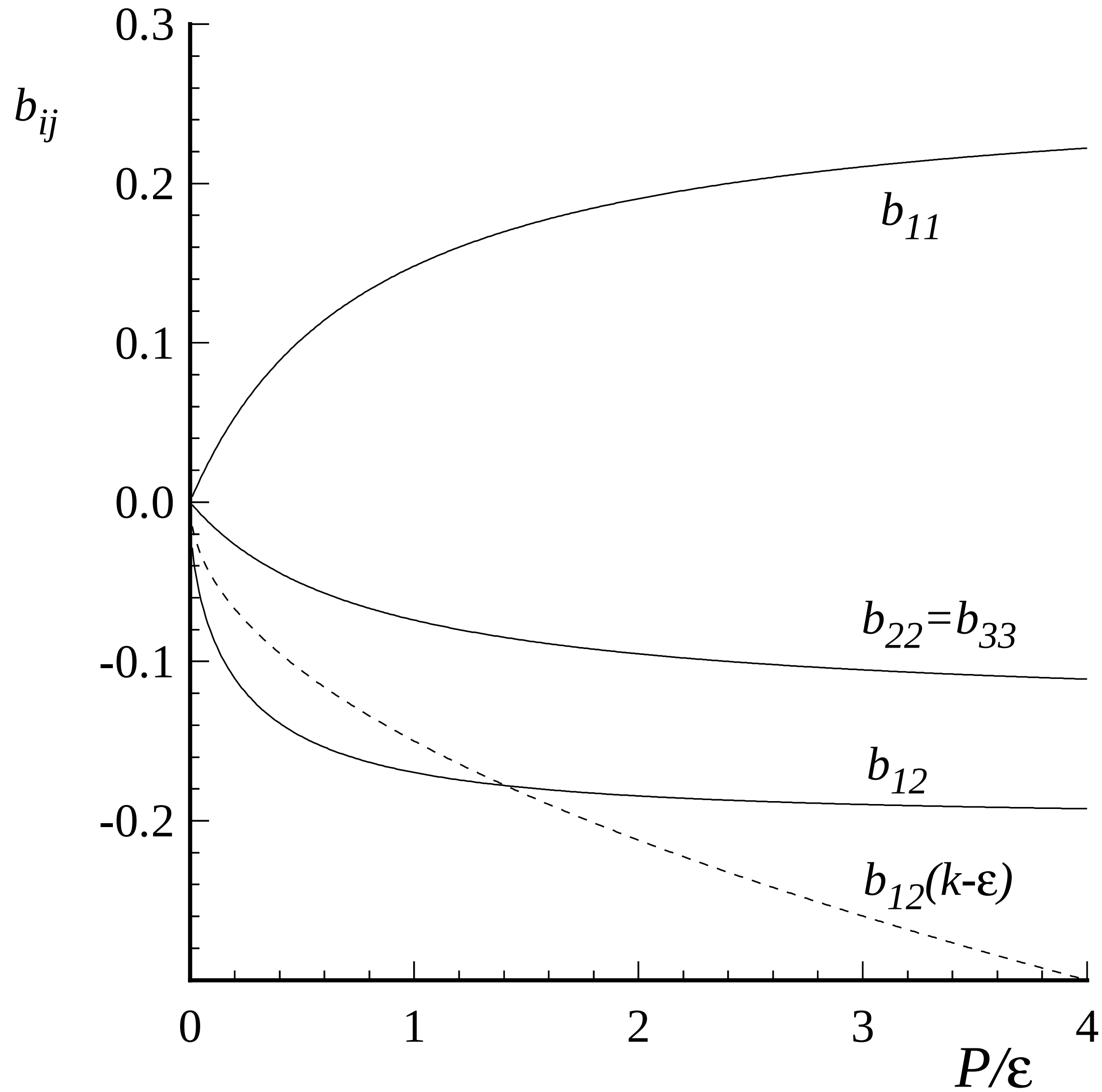

Figure 11.20: Reynolds-stress anisotropies as functions of $\mathcal{P}/\varepsilon$ according to the LRR-IP algebraic stress model. The dashed line shows b_{12} according to the k-ε model.

Turbulent Flows

Stephen B. Pope
Cambridge University Press, 2000

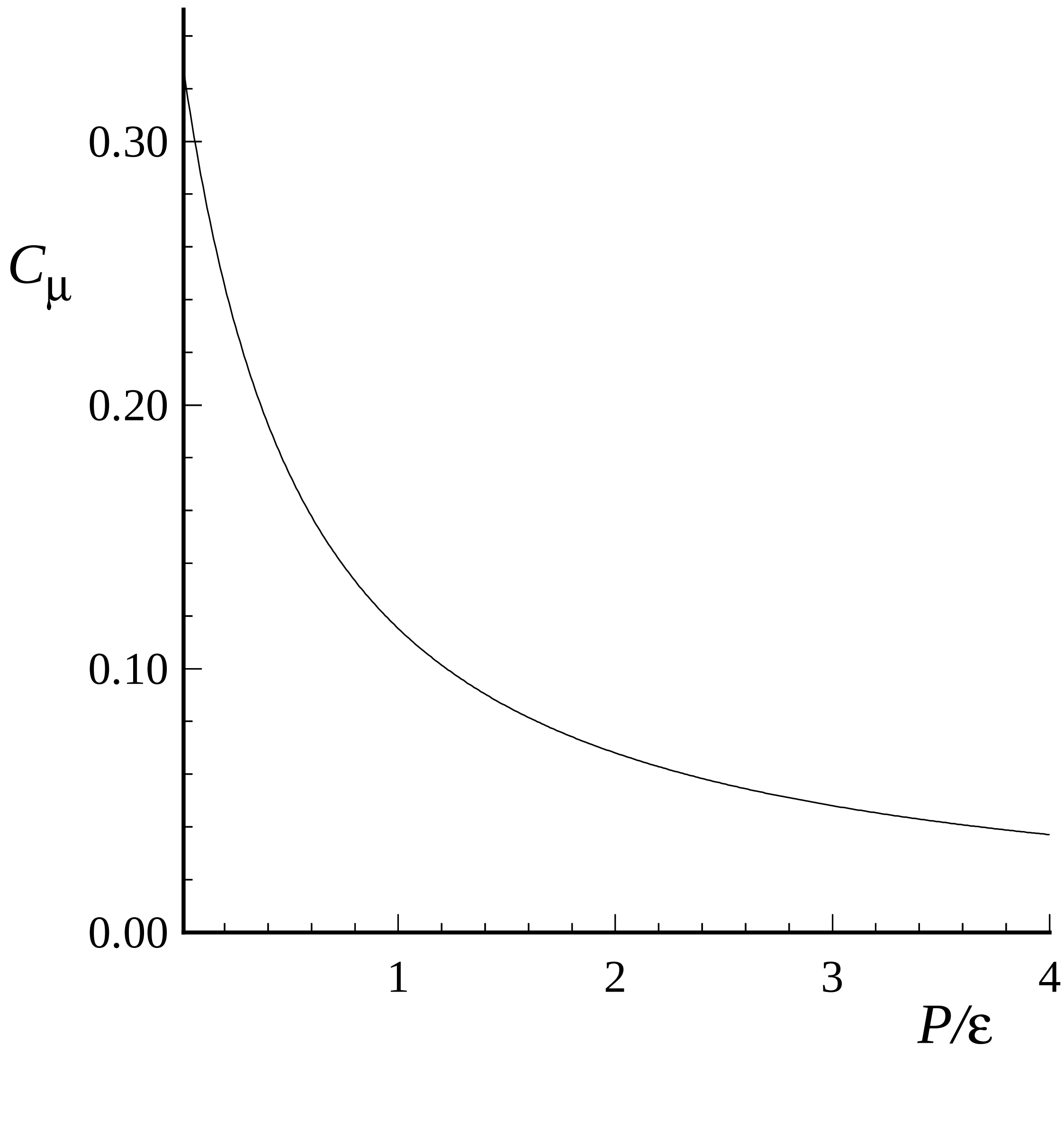

Figure 11.21: The value of C_μ as a function of $\mathcal{P}/\varepsilon$ given by the LRR-IP algebraic stress model (Eq. 11.220).

Turbulent Flows

Stephen B. Pope
Cambridge University Press, 2000

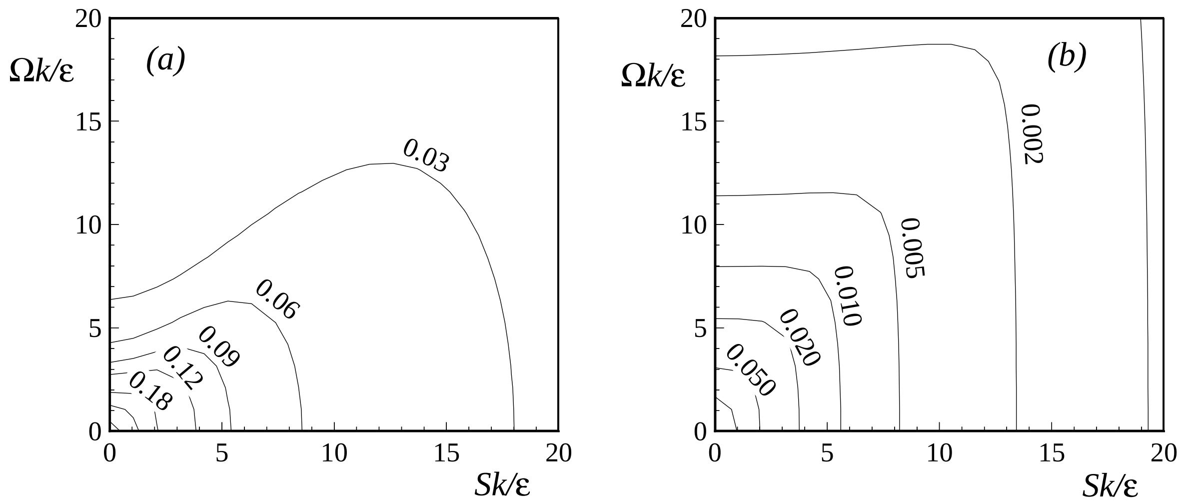

Figure 11.22: Contour plots of (a) $C_\mu = -G^{(1)}$, and (b) $-G^{(2)}$, for the LRR-IP nonlinear viscosity model (Eqs. 11.230–11.232).